Experimental and Numerical Study of SRG-to-Masonry Joints

Salvatore Verre[1], Sam Cocking[2], Alessio Cascardi[3], Raimondo Luciano[4], Francesco Fabbrocino[5], and Carlo Olivieri[5(✉)]

[1] Department of Theoretical and Applied Sciences (DiSTA), eCampus University, Novedrate Como, Italy, via Isimbardi 10, Novedrate, CO, Italy
[2] Department of Engineering, Cambridge, UK
[3] Department of Civil Engineering, University of Calabria, Arcavata di Rende, Italy
[4] Parthenope University, Naples, Italy
[5] Department of Engineering, Pegaso Telematic University, Centro Direzionale ISOLA F2, Naples, Italy
carlo.olivieri@unipegaso.it

Abstract. Steel reinforced grout (SRG) – in which steel fiber strips are embedded in an inorganic mortar – is a promising strengthening methodology for the retrofitting of reinforced concrete (RC) or masonry structures. While its effectiveness has been established in various applications, delamination (debonding) at the fiber-mortar or mortar-substrate interfaces may dramatically affect its mechanical performance when a premature failure occurs. Bond tests can provide crucial insights by evaluating debonding forces versus slip relationships. The performance of SRG interventions depends on factors including the fiber and mortar types, reinforcement layers, bonded length, substrate properties, and environmental conditions. To address the current lack of knowledge regarding these criteria, this paper presents experimental and numerical studies of SRG-to-masonry bonds. Specifically, Finite Element (FE) analysis is used to model typical SRG-to-masonry joints, leveraging results from a previous campaign of laboratory tests. The results showed satisfactory accuracy of the experimental/numerical comparison, in terms of constitutive bond laws.

Keywords: FRCM · SRG · Masonry · shear bond tests · Finite Element Model FEM

1 Introduction

Unreinforced masonry buildings offer a good structural capacity when they have been well designed [1–12], even when currently in a deformed configuration due to external boundary conditions [13–16], or in the case of slender structures [17]. However, due to damage or mechanical decay to the masonry over time, strengthening may become necessary [18]. Enhancing existing structures, to enable their life extension or reuse with increased load-carrying capacity, has led to a growing interest in composite materials for strengthening. These materials, with reinforcing fibers in organic or inorganic

© The Author(s), under exclusive license to Springer Nature Switzerland AG 2026
O. Gervasi et al. (Eds.): ICCSA 2025 Workshops, LNCS 15886, pp. 302–313, 2026.
https://doi.org/10.1007/978-3-031-97576-9_20

matrices, are bonded to structures to increase performance with minimal invasiveness. Fiber Reinforced Polymers (FRP), Fabric Reinforced Cementitious Matrices (FRCM) and Steel Reinforced Grout (SRG) are among the most popular composite systems used for structural strengthening. Their mechanical performance is dependent on the interaction between the reinforcing fibers and the matrix [19, 20]. In particular, SRG consists of galvanized high-strength steel wires twisted together to form cords that can be arranged at different distances from each other, obtaining different specific density levels [21]. In this way, unidirectional fabrics are created. The diameter of the steel wires ranges from 0.1 to 0.5 mm, and coatings are used to prevent corrosion. This manufacturing approach leads to cord tensile strengths between 2800 and 3200 N/mm^2, with Young's moduli between 180 and 210 N/mm^2. Variation of the cord spacing results in different densities. Typical overall density values for low (LD), medium (MD), and high (HD) density SRG are 600 g/m^2, 2000 g/m^2, and 3300 g/m^2, respectively.

Recent experimental investigations have studied the mechanical behavior of structural members strengthened in shear [22] or confined [23] with SRGs. The results clearly indicate debonding processes that may occur at both the fiber-mortar and mortar-substrate interfaces. These processes can be analyzed in greater detail by bond tests, including either single- or double-lap direct shear tests. These enable evaluation of local debonding forces, slip laws, and corresponding interface fiber stresses. However, experimental investigations on SRG-to-masonry bond behavior are rarer [24–27], reporting on single-lap shear tests with varying bonded lengths and loading rates.

These tests observed failures occurring through fiber rupture, mixed mode failure, de-bond of the masonry-matrix interface, and inter-laminar failure between the fibers and matrix. The failure type was primarily influenced by the bonded length which, in these tests, varied between 175 and 200 mm. However, high dispersion of textile-to-matrix slippage measurements was also observed. This was ascribed to factors including the non-homogeneous stress distribution among the steel cords and within the filaments in each cord, cords-to-matrix friction, and failure mode developments.

Ascione et al. [26] conducted an extensive experimental study on the bond behavior between SRG and concrete. These tests investigated the influence of the surface roughness of the concrete, the density of the steel fibers (including both LD and MD fiber spacings), the bonded length, and the concrete strength. Failures in the SRG matrix were observed due to both sliding phenomena and cohesive failure, irrespective of strength or surface roughness of the underlying concrete specimens. While the use of a higher number of steel strips in the SRG was correlated with an improved maximum load capacity, a reduced average tensile strength (and hence exploitation ratio) was also observed. The effective bonded length in these tests was between 200 and 300 mm, for the LD and MD steel fibers, respectively.

Additionally, Sneed et al. [27] performed shear bond tests to evaluate the bond performance between SRG composites and concrete. The SRG composites were constructed using MD steel fibers and a mineral mortar. A bonded length of 330 mm was used in these tests, which were performed both with and without an external mortar layer. Failures of the fibers occurred either by slippage within the matrix or direct fracture. There was no post-peak softening seen in the load response.

Beyond the parameters studied to date in the literature, others may influence the behaviour of SRG-reinforced structures. These include the precise specifications of the fiber and mortar types, the number of reinforcement layers, the preparation used for the external substrate, its strength, and environmental conditions. Further work is needed to study the effects of these parameters before a reliable analytical model can be developed for the overall performance of SRG-reinforced structures.

In this paper, numerical and experimental studies on SRG-to-masonry bonds are presented and discussed. Specifically, a series of direct, single-lap shear tests were performed on SRG-reinforced brick masonry specimens. A numerical Finite Element (FE) procedure was then developed, utilizing the well-recognized FE software [28], to predict the global behavior of SRG-to-masonry joints. The following sections outline the experimental and numerical procedures used in this study, before a discussion of the key results and potential avenues for future research.

2 Experimental Investigation

2.1 Materials and Specimen Preparation

Three single-lap shear tests were performed at the University of Calabria laboratory using a push-pull configuration. For full details of these tests, see [29]. Each masonry specimen had cross-sectional dimensions of 120 × 120 mm, a joint length of 510 mm, and was constructed using eight clay bricks. The average brickwork compressive strength, $f_{bc} = 42$ MPa (with a coefficient of variance of 0.0526), was measured by coring four samples of 50 × 50 mm cross section from bricks in the same batch used to build the test specimens. The masonry test specimens were constructed and strengthened with SRG in laboratory conditions. The fiber fabric density of the steel used for SRG reinforcement was 1200 g/m^2. and the cross-sectional area of each cord was 0.538 mm^2 (Fig. 1). The steel fiber consisted of micro cords, each comprising five filaments. Two filaments were used to wrap the remaining three to create each micro cord.



Fig. 1. Medium steel mesh used in SRG reinforcement.

Tensile tests on five typical coupons were used to determine the mechanical properties of the fiber mesh, using the experimental setup shown in Fig. 2a. The length and width of each coupon were 560 mm and 50 mm, respectively. The coupon cross section contains

eight steel cords, giving a resultant area of $A_f = 4.30$ mm^2. The ends of each coupon were fixed to thin steel plates measuring 80 mm in length. The displacement rate for these testss was 1.25 mm/s, and axial strain was recorded using an extensometer of gauge length = 50 mm. Results for the elastic modulus, tensile strength, and ultimate strain are presented in Table 1, while Fig. 2b shows the experimental stress–strain curves.

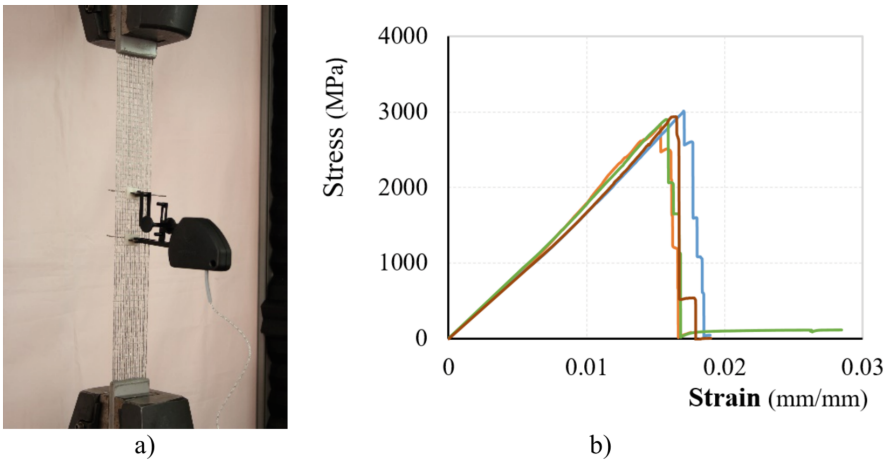

Fig. 2. A) Coupon test setup and b) resulting stress–strain curves.

Table 1. Steel fibre geometry and measured mechanical properties.

	Steel fiber
Elastic modulus	*200 GPa (8%)*
Break deformation	0.020 mm/mm (8%)
Equivalent thickness	*0.169 mm*

To reinforce the masonry specimens, the steel fibers were embedded between two, 5 mm-thick matrix layers and bonded to the specimens, beginning 30 mm from the edge of the top surface. A mold was used to ensure uniform thickness of the composite strip.

3 Results and Numerical Model

This paper presents the results for three specimens, which were subjected to classical, push-pull tests. In these, fibers were pulled while the masonry joint remained fixed in place. Aluminum load tabs were used to apply force to the top of the fibers, while a 100 kN load cell was used to perform measurements. The tab width was identical to that of the specimens (50 mm), while their length was 60 mm. Even attachment to the bare fiber was achieved using epoxy resin, ensuring uniform distribution of pressure

during the test. Slip was calculated by averaging recordings from two linear variable displacement transducers (LVDTs), labeled "*a*" and "*b*" (c.f., Fig. 3). These LVDTs were located near to the bonded region of the specimens. The displacement rates for these tests was 0.18 mm/min. Figure 3 shows the experimental setup.

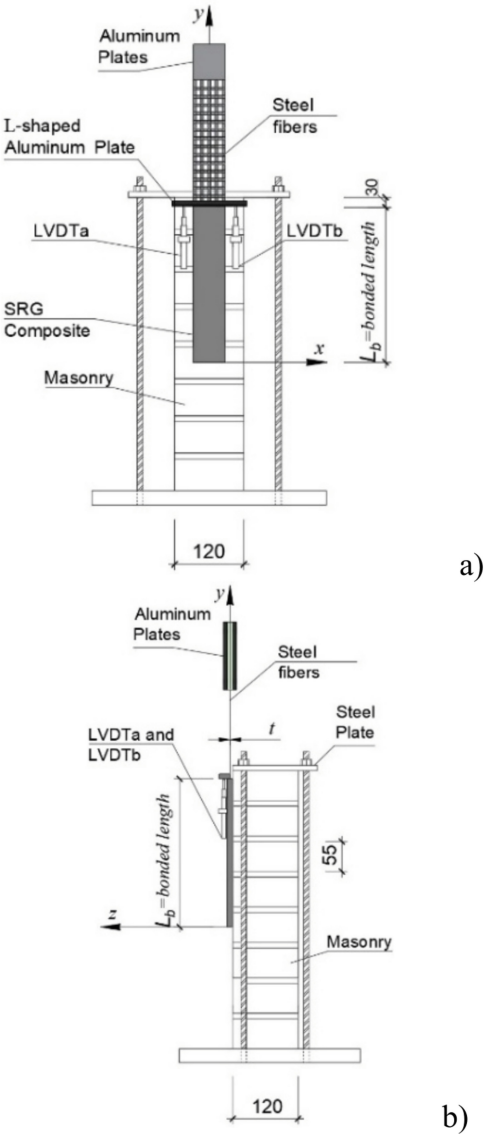

Fig. 3. Experimental setup for the single-lap shear tests: a) front and b) side views.

The naming convention for the test specimens was "*DS_N*," in which "*N*" denotes the specimen number. Table 2 summarizes the maximum applied load (P_{max}) achieved in each test.

Table 2. Maximum applied loads in the direct shear tests.

	P_{max} [kN]	Average [kN]
DS_1	*6.46*	*6.04*
DS_2	*5.32*	
DS_3	*6.35*	

3.1 Geometrical Modelling and Materials Model

Two modelling techniques were used in the numerical procedure, in the FE software. First, the masonry substrate was modeled using 3D FE elements (C3D4) for macro modeling [30, 31], while the steel fibers and the inorganic mortar were modeled using 2D shell elements (S4). The 3D element presents a tetrahedral geometry with 4 nodes, and was characterized by linear interpolation functions and constant stress. However, 2D shell elements were quadrilinear and presented a membrane strain and a reduced integration with hourglass control. In Fig. 4, the adopted FE mesh is shown. This was obtained after mesh sensitivity analysis, aimed to avoid mesh influence on the results. Vertical and horizontal displacements at the base of the masonry prism were constrained, as well as for the horizontal displacements at the top (*y-z plane*).

The nonlinear behavior of the inorganic matrix was described using the Concrete Damage Plasticity model (CDP). This function is commonly used in the literature, to model the quasi-brittle materials found in masonry or concrete elements [32]. CDP is essentially an extension of the Drucker–Prager model, featuring a modified yield criterion. In the CDP model, the hardening/softening strain branch is influenced by the potential function parameter, which can be set equal to or different from the frictional parameter. The steel fibers were modeled as a homogeneous elastic material up to failure. The input parameters included the density ($\rho = 2.5$ g/cm^3), the elastic modulus as evaluated in Sect. 2.1, and the Poisson's ratio ($\nu = 0.3$).

3.2 Interface Modelling

In SRG systems, debonding is frequently observed at the fibre-mortar interfaces. Assuming that this will be the site of failure, interactions at the substrate-matrix interface are modeled as perfectly bonded. In contrast, interface conditions at the fiber-matrix interfaces (for both the internal and external matrices) were modeled as a cohesive surface through general contact. These contact surfaces are critical components of the SRG system, and are shown in Fig. 5. Relative displacements occurring at these interaction

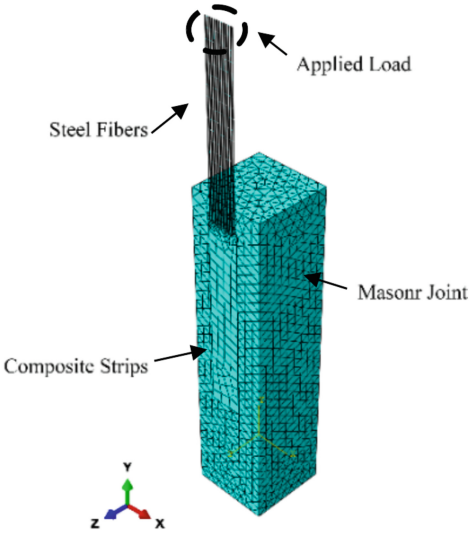

Fig. 4. Geometrical modeling and FE analysis

surfaces are described using the "traction-separation approach" (as specified in the software), applied to these contact surfaces. This internal function follows a bilinear pattern, with an initial linear elastic response followed by softening. The softening phase captures damage progression.

The bond-slip law used in this study is based on the bilinear model proposed in [33] for FRP composites (Fig. 6). This approach utilizes a bilinear function to capture Mode I and Mode II failure modes, as well as the initiation and progression of damage. Initiation of damage occurs at the peak of normal or shear stress. The adopted bond-slip law consists of three linear branches [33] and was proposed for analyzing FRP–concrete joints. Since the load-slip responses of both FRP and SRG systems are similar, the same bond-slip law can be used to analyze the performance of structures reinforced with SRG. The parameters were calibrated specifically for SRG composites using experimental data, resulting in the following estimates: initial stiffness $k_0 = 77.01$ N/mm^3, bond stress reaches $\tau_{max} = 5.93$ MPa, and Fracture Energy $G_f = 0.67$ N/mm.

3.3 Computational Results

The numerical simulations again assumed displacement control conditions for the load tests. Specifically, an enforced displacement (λ_d) was imposed at the top surface of the steel fibers. To obtain nonlinear numerical solutions, a dynamic (i.e., *explicit*) approach was employed. This method is commonly used for quasi-static analyses that involve complex nonlinear effects and contact conditions. Consequently, direct integration of the governing equation of motion was possible using an extended Newmark *β-method*, known as the *Hilber-Hughes-Taylor (HHT)* time-integration operator. It is important to note that the model consists of multiple components (substrate, matrix, and fabric) with different stiffness and mass properties.

These components are addressed separately in the numerical dynamic solution using a scaling method. The main parameters for obtaining the static solution include variable mass scaling, alongside the ratio of kinetic and internal energies. In this study, a variable mass scaling of 0.00005 was applied throughout, and the ratio was constrained below 5% throughout analysis.

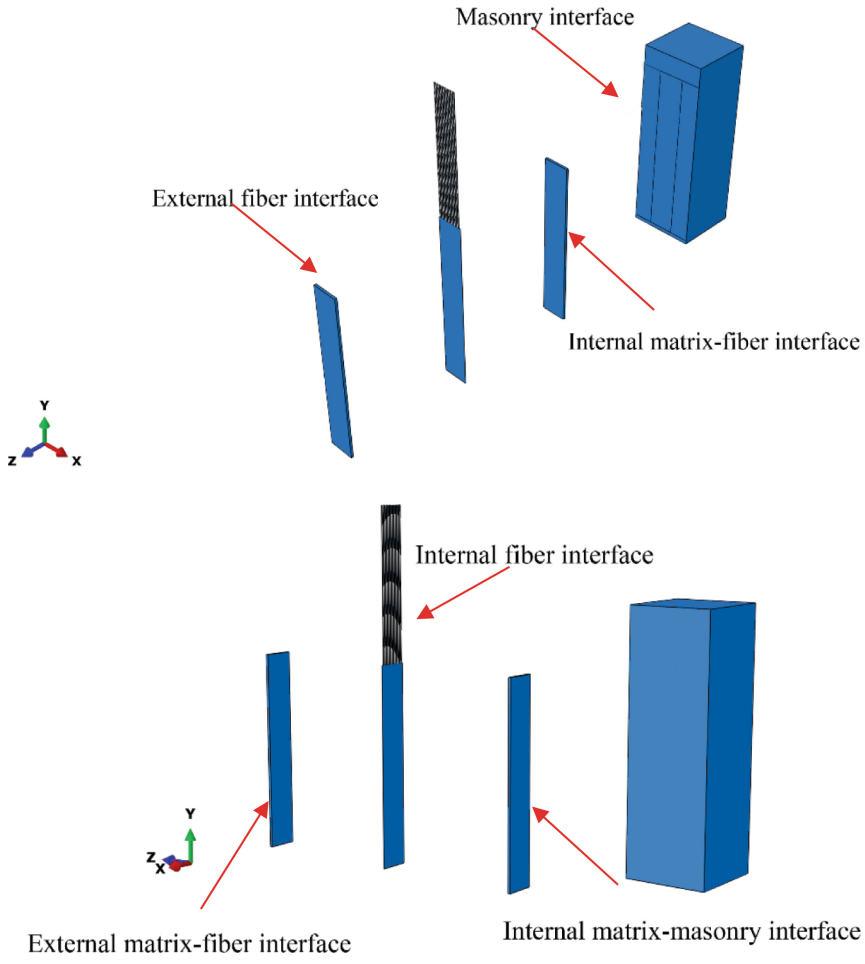

Fig. 5. Interaction surfaces

3.4 Result and Discussion

Figure 7 shows the typical failure mode, while Fig. 8 presents results obtained for the direct shear tests. Initially, the load-response curve (Fig. 8) exhibits a linear segment, corresponding to linear-elastic bond behavior at the fiber-matrix interface. Following this,

increases in global slip led to a nearly uniform applied load until sudden failure, characterized by softening in the response. During this stage, micro-damage was observed at the fiber-matrix interfaces.

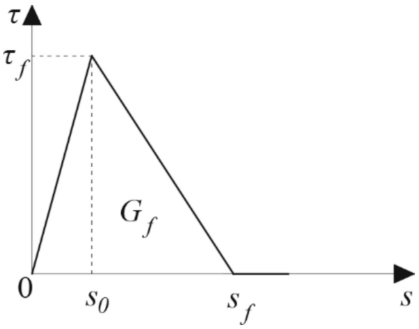

Fig. 6. Bond slip law



Fig. 7. Typical failure mode

The numerical results, as shown in Fig. 8, align well with the experimental data. However, the numerical model slightly underestimated the maximum applied load, reporting a value of 5.73 kN, which corresponds to a 6% error (Fig. 8).

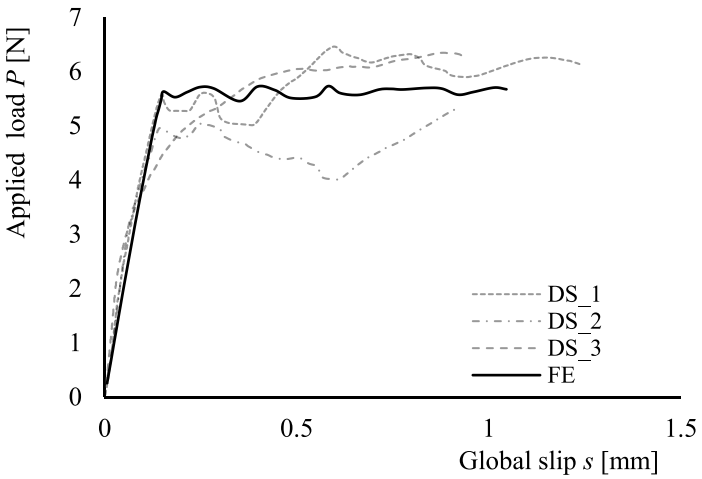

Fig. 8. Comparison of experimental and numerical curves of applied load, P, vs. global slip, s.

4 Conclusions

This paper summarizes results from parallel experimental and numerical studies of the stress-transfer behaviour and matrix-fiber interface performance for masonry substrates reinforced using SRG systems. The following key findings have been observed:

- Debonding of the matrix-fiber interfaces is the key driver of failure, resulting in complete separation and loss of the external reinforcing layer.
- The MD SRG system used in this study has proven to be effective as an avenue for strengthening retrofit. Further details of the performance of this MD SRG system can be found in [29].
- The numerical FE simulations provided a satisfactory prediction of the maximum applied load, and hold promise for prediction of general SRG behaviour.

However, the results obtained are valid only for the tested strengthening system, as variations in fiber sheet density and inorganic matrix can occur with different substrates. Therefore, further experimental investigations are needed to validate these findings, specifically examining the influence of other variables. These variables of interest include the number of steel textile layers used in the reinforcement, the masonry substrate strength, and the curing conditions of the mortar.

Acknowledgments. The authors are grateful for the following financial support from the Italian Ministry of University and Research (MUR): Research Grant PRIN 2020 No. 2020EBLPLS on "Opportunities and challenges of nanotechnology in advanced and green construction materials"; and Research Grant PRIN 2022 No. 2022TN5M7F on "TReE - Supporting the Transition to Ecological Economy in Italian cities Regeneration: circular model tools for reusing architecture and infrastructures".

References

1. Olivieri, C., Fortunato, A., DeJong, M.: A new membrane equilibrium solution for masonry railway bridges: The case study of Marsh Lane Bridge. Int. J. Masonry Res. Innov. **6**(4), 446–471 (2021)
2. Olivieri, C., Adriaenssens, S., Cennamo, C.: A novel graphical assessment approach for compressed curved structures under vertical loading. Int. J. Space Struct. **38**(2), 141–155 (2023)
3. Buonocore, G., Gesualdo, A., Monaco, M., Savino, M.T.: Improvement of Seismic Performance of Unreinforced Masonry Buildings using Steel Frames, In: Civil-Comp Proceedings: 106, B.H.V. Topping and Iványi eds., Civil Comp Press, Kippen, Stirlingshire, U.K (2014)
4. Gesualdo, A., Monaco, M.: Seismic vulnerability reduction of existing masonry buildings. Modelling of retrofitting tecniques. In: Urban Habitat Construction Under Catastrophic Events. 1, 853–858, London, New York: CRC Press, Taylor & Francis Group (2010)
5. Gesualdo, A., et al.: Seismic retrofitting techniques for masonry arch bridges. Urban Habitat Constr. Catastrophic Events. **1**, 859–864 (2010)
6. Olivieri, C.: FORMERLY-Math: constrained form-finding through membrane equilibrium analysis in Mathematica. Software Impacts **16**, 100512 (2023)
7. Crespino, E., Adriaenssens, S., Fraddosio, A., Olivieri, C., Piccioni, M.D.: A multi-objective optimization approach for novel shell/frame systems under seismic load. Struct. **65**, 106625 (2024)
8. Di Gennaro, L., de Cristofaro, M., Loreto, G., Minutolo, V., Olivares, L., Zona, R., Frunzio, G.: In-situ load testing of an ancient masonry structure using fibre optics. Structures, **70** (2024)
9. Iannuzzo, A., Montanino, A.: A limit analysis-based CASS approach for the in-plane seismic capacity of masonry façades. Int. J. Solids Struct. **289**, 112633 (2024)
10. Fabbrocino, F., Olivieri, C., Luciano, R., Vaiano, G., Maddaloni, G., Iannuzzo, A.: Seismic performance of historic masonry buildings: A comparative analysis of equivalent frame and block-based methods. Alex. Eng. J. **109**, 359–375 (2024)
11. Olivieri, C., Cocking, S., Fabbrocino, F., Iannuzzo, A., Placidi, L., Adriaenssens, S.: Seismic capacity of purely compressed shells based on Airy stress function. Continuum Mech. Thermodyn. **37**(2), 21 (2025)
12. Iannuzzo, A., Mallardo, V.: A novel approach to model differential settlements and crack patterns in masonry structures. Eng. Struct. **323**, 119220 (2025)
13. Pingaro, N., Milani, G.: Simple non-linear numerical modelling of masonry arches reinforced with SRG using elasto-fragile and elasto-ductile truss finite elements. Eng. Struct. **293**, 116637 (2023)
14. Iannuzzo, A., Musone, V., Ruocco, E.: A neural network-based automated methodology to identify the crack causes in masonry structures. Comput.-Aided Civil and Infrastructure Eng. **39**(24), 3769–3785 (2024)
15. Montanino, A., Iannuzzo, A.: A quadrilateral plate-type finite element to model stress singularities in no-tension materials. Comput. Methods Appl. Mech. Eng. **432**, 117433 (2024)
16. D'Altri, A.M., de Miranda, S., Castellazzi, G., Glisic, B.: Numerical modelling-based damage diagnostics in cultural heritage structures. J. Cult. Herit. **61**, 1–12 (2023)
17. Di Gennaro, L., Guadagnuolo, M., Monaco, M.: Rocking Analysis of Towers Subjected to Horizontal Forces. Build. **13**(3) (2023)
18. Massaro, L., Di Gennaro, L., Guadagnuolo, M., Frunzio, G.: Strengthening of Masonry Arches: The "Santa Maria delle Grazie" Church. COMPDYN Proceedings (2023)
19. Carloni, C., Verre, S., Sneed, L.H., Ombres, L.: Open issues on the investigation of PBO FRCM-Concrete debonding. Compos. Struct. **299** (2022)

20. Ombres, L., Aiello, M.A., Cascardi, A., Verre, S.: Modeling of Steel-Reinforced Grout Composite System-To-Concrete Bond Capacity Using Artificial Neural Networks. J. Compos. Constr., **28**(5) (2024)
21. Sneed, L.H., Verre, S., Ombres, L., Carloni, C.: Flexural behavior RC beams strengthened and repaired with SRP composite. Eng. Struct. **258** (2022)
22. Ombres, L., Verre, S.: Influence of the strengthening configuration on the shear capacity of reinforced concrete beams strengthened with SRG (steel-reinforced grout) composites. Fibers **10**(7), 57 (2022)
23. Aiello, M.A., et al.: Masonry columns confined with fabric reinforced cementitious matrix (FRCM) systems: A round robin test. Constr. Build. Mater. **298** (2021)
24. Santandrea, M., Focacci, F., Mazzotti, C., Ubertini, F., Carloni, C.: Determination of the interfacial cohesive material law for SRG composites bonded to a masonry substrate. Engineering Failure Analysis, **111** (2020)
25. Bencardino, F., Nisticò, M., Verre, S.: Experimental Investigation and Numerical Analysis of Bond Behavior in SRG-Strengthened Masonry Prisms Using UHTSS and Stainless-Steel Fibers. Fibers 2020, **8**(8), (2020)
26. Ascione, F., Lamberti, M., Napoli, A., Realfonzo, R.: Experimental bond behavior of Steel Reinforced Grout systems for strengthening concrete elements. Constr. Build. Mater. **232**, 117105 (2020)
27. Sneed, L.H., Verre, S., Carloni, C., Ombres, L.: Flexural behavior of RC beams strengthened with steel-FRCM composite. Eng. Struct. **127**, 686–699 (2016)
28. Abaqus Theory and User's Manual: Version 2025
29. Ombres, L., Iorfida, A., Verre, S.: FRCM/SRG - Masonry Joints: Experimental Investigation and Numerical Modelling. Key Eng. Mater. **817**, 3–8 (2019)
30. Verre, S.: Numerical Strategy for Column Strengthened with FRCM/SRG System. Build. **12**, 2187 (2022)
31. Pingaro, N., Milani, G.: Non-linear 1D 16-DOF finite element for Fiber Reinforced Cementitious Matrix (FRCM) strengthening systems. Comput. Struct. **300**, 107422 (2024)
32. John, S. K., Cascardi, A., Verre, S., Nadir, Y.: RC-columns subjected to lateral cyclic force with different FRCM-strengthening schemes: experimental and numerical investigation. Bullet. Earthquake Eng. 1–30 (2025)
33. Lu, X.Z., Teng, J.G., Ye, L.P., Jiang, J.J.: Bond slip models for FRP sheet/plates bonded to concrete. Eng. Struct. **27**(6), 920–937 (2005)